Organogels

Self-Replenishable Anti-Waxing Organogel Materials**

Xi Yao, Shuwang Wu, Lie Chen, Jie Ju, Zhandong Gu, Mingjie Liu, Jianjun Wang,* and Lei Jiang

Abstract: *Solid deposition, such as the formation of ice on outdoor facilities, the deposition of scale in water reservoirs, the sedimentation of fat, oil, and grease (FOG) in sewer systems, and the precipitation of wax in petroleum pipelines, cause a serious waste of resources and irreversible environmental pollution. Inspired by fish and pitcher plants, we present a self-replenishable organogel material which shows ultra-low adhesion to solidified paraffin wax and crude oil by absorption of low-molar-mass oil from its crude-oil environment. Adhesion of wax on the organogel surface was over 500 times lower than adhesion to conventional material surfaces and the wax was found to slide off under the force of gravity. This design concept of a gel with decreased adhesion to wax and oil can be extended to deal with other solid deposition problems.*

Wax deposition in industrial petroleum pipelines is a worldwide problem and pipeline blockage and breach caused by wax deposition causes serious environmental pollution and billions of dollars of financial loss every year.[1] To address this problem, great efforts have been devoted to predicting the formation of wax deposits along pipelines[2] and developing different methods including the use chemical additives,[3] heating stations, and mechanical pigging[4] to remove the detected wax blockages. Unfortunately, these methods are either time or energy consuming. It is highly desirable to remove the solidified wax deposited on the pipeline surface

by taking advantage of the flowing crude oil in the pipelines. To achieve this, the key is to decrease the adhesion of solidified wax to the pipeline surface.

Inspired by pitcher plants, T.-S. Wong and J. Aizenberg et al. developed liquid-repellent surfaces, namely slippery liquid-infused porous surfaces (SLIPS).[5] SLIPS have since been explored for a variety of applications, such as liquid-drop manipulation,[6] fog harvesting,[7] and in anti-icing.[8] The theoretical criteria to prepare SLIPS have been reported by A. Lafuma and D. Quéré.[9] It should be noted that as a typical artificial material, the stability of the lubricant against harsh environments, such as ice and a powerful liquid flow, is still a concern.[10] In nature, both fish[11] and pitcher plants[12] show excellent and sustainable anti-adhesion properties against foreign bodies when their surfaces are subjected to humid environments. The lubricant film is self-replenishing because fish and pitcher plants obtain water lubricant from their vicinity. Inspired by this, we report herein a self-replenishable organogel (OG) material with sustainable ultra-low adhesion to the paraffin wax solidified on its surface. The shear stress necessary to remove the solidified paraffin wax on the OG surface is as low as 0.5 kPa, which is hundreds of times lower than that required to remove wax on the surface of materials typically used in conventional pipelines, such as steel (162.3 kPa) and plastics (186.6 kPa). More importantly, the low adhesive properties of the surface can be sustainable because the absorbed lubricant is provided by the crude oil itself in the form of low-molar-mass compounds.

As shown in Figure 1 A, the OG can be simply obtained by immersing cross-linked poly(dimethylsiloxane) (PDMS) in crude oil (or petroleum products such as gasoline, diesel oil, or *n*-alkanes) for one day. After this time, it was observed that the as-prepared OG material had become larger in size than its PDMS starting material (Figures 1 A, B). Note, although PDMS was used for demonstration, other cross-linked elastomers showing a certain oil affinity could also be used to prepare the OG material.[13] It has been established that the interaction between a solvent and the cross-linked polymer network can be quantified as:[14]

$$D_c^s = kT/6\pi\eta_s\xi_H \tag{1}$$

where D_c^s is the cooperative diffusion coefficient which correlates with the swelling degree of the cross-linked network, k is the Boltzmann constant, T is the absolute temperature, η_s is the viscosity of the solvent, and ξ_H can be taken as the polymer chain length between adjacent cross-linking points. Guided by Equation (1), we examined the dependence of the swelling ratio on the molar mass of the absorbed oil, the cross-linking density of PDMS, and the chemical composition of the cross-linked silicone (see Figures S1–S3 in the Support-

[*] Dr. X. Yao, S. Wu, Dr. J. Ju, Prof. J. Wang, Prof. L. Jiang
Beijing National Laboratory for Molecular Science (BNLMS)
Institute of Chemistry, Chinese Academy of Sciences
Beijing, 100190 (P.R. China)
E-mail: wangj220@iccas.ac.cn

Dr. X. Yao
College of Chemistry, Jilin University
Changchun, 130012 (P.R. China)

Dr. L. Chen, Dr. Z. Gu, Prof. M. Liu
Key Laboratory of Bio-inspired Smart Interfacial Science and
Technology of Ministry of Education, School of Chemistry and
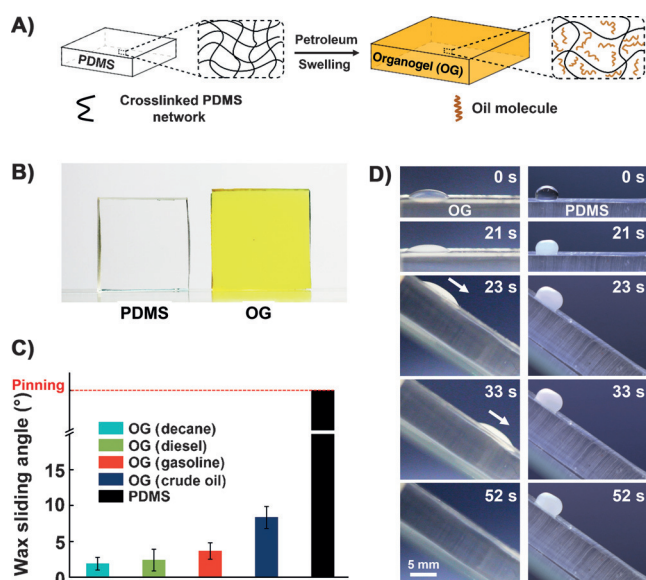Environment, Beihang University, Beijing, 100191 (P.R. China)

Supporting information for this article is available on the WWW under http://dx.doi.org/10.1002/anie.201503031.

Figure 1. A) PDMS was immersed in petroleum, resulting in the diffusion of oil molecules into the cross-linked PDMS network and swelling of the PDMS. B) The resulting OG was transparent and larger in size (circa 2.2×2.2 cm^2) than the as-prepared PDMS (approximately 2×2 cm^2) because of the swelling. C) The low sliding angle of the solidified paraffin wax on the OG swollen by different petroleum products (given in parentheses) showing ultra-low wax/OG adhesion, whereas wax solidified on the PDMS surface was firmly adhered (pinned). D) Comparison of the adhesion of solidified paraffin wax deposited on OG (left) and PDMS (right) surfaces.

ing Information for experimental details). The results are in good agreement with the prediction calculated by using Equation (1). Additionally, the yellow and transparent OG shown in Figure 1B suggests that the crude oil absorbed in the cross-linked network is mainly the fraction with low-molar-mass components (such as kerosene and diesel). This conclusion is further validated by GC–MS analysis (Figure S4), which shows that the oil content in the OG network mainly consists of paraffins with numbers of carbon atoms ranging from 9 to 21. As a consequence, there is only a trace amount of wax crystals in the OG network at low temperature (Figure S5). This is consistent with Flory–Huggins solution theory,[15] where entropy gain dominates the swelling of the cross-linked silicone, thus the swelling capability of low-molar-mass components from the crude oil into the OG is better than those of high-molar-mass components.

Figure 1C shows the sliding angle (θ) of the solidified paraffin wax (defined as the tilting angle of the surface at which the solidified paraffin wax starts to slide) on the surface of the OG swollen by different oils. The wax sliding angle was found to be less than 10° regardless of the type of oil used, meaning that the force needed to remove a solidified paraffin wax is less than one fifth ($\sin 10° < 0.2$) of the paraffin wax's gravity. Conversely, the solidified paraffin wax stuck firmly on the non-swollen PDMS surface. When a gel material is saturated with a good solvent, its surface tends to be suffused by the solvent, an occurrence driven by osmotic pressure.[16] The featured asymmetric AFM force curve[17] shown in Figure S6 verifies the existence of a thin liquid layer above

the solid silicone surface. Figure 1D demonstrates the sliding motion of the solidified paraffin wax on the OG surface and pure PDMS surface with increasing time (see also Movie S1 and S2 in the Supporting Information). When the melted paraffin wax (C$_{24}$H$_{50}$, m.p. ≈ 50°C) was deposited on the OG surface at room temperature, it spread and became opaque. After 21 s, the OG was tilted by 37° and the solidified paraffin wax slid down along the OG surface and finally went out of the window of the camera at 52 s. However on PDMS surface, the solidified paraffin wax was stuck where it had been deposited, indicating that paraffin wax tends to firmly adhere onto the solid surface. It should be noted that in reality, the contact time of the crude oil with the solid surfaces is much longer. Therefore, experiments employing a longer contact time of the solid surfaces with the liquid paraffin wax before solidification and investigating the adhesion of the solidified wax with the organogel were undertaken (see the Supporting Information). We demonstrated in Figure S7 that a solidified paraffin wax can slide off the OG surface purely under its own gravity (see also Movies S3 and S4).

To explain this low adhesion, environmental scanning electron microscopy (ESEM) was used to investigate the morphology of the solidified paraffin wax surface which had been in contact with the OG surface. Figure 2A shows the microscale structure formed on the solidified paraffin wax surface. The proposed structure is shown schematically in Figure 2C. When the liquid paraffin wax at higher temperature (80°C) approaches the OG surface at lower temperature (25°C), it first meets the thin oil layer atop the OG. Subsequently, the liquid paraffin wax diffuses into the thin oil layer and forms a diffusion layer. When wax nucleation occurs, it begins at the wax-rich location,[18] and so nucleation at the PDMS surface is prevented. The growth of the wax crystals consumes the paraffin wax in the diffusion layer and finally forms a microscale structure. A similar wax structure was detected for a longer time of contact between wax and the OG (Figure S8), indicating the existence of a diffusion balance between the two compounds. Similar microscale structures of paraffin wax have been reported.[19]

The formation of this unusual structure has two consequences. First, the solid/solid contact area is largely decreased. Second, the voids in the structures are filled with the oil. Consequently, the liquid layer acted as a lubricant which resulted in solid/liquid/solid contact. Figure 2B shows the smooth surface morphology of paraffin wax solidified on the nonswollen solid surface. As shown in Figure 2D, similar to the actual occurrence in petroleum transport,[20] heterogeneous wax nucleation is initiated at the solid surface. Consequently, the growing wax crystal is formed in the shape of indentations and features of the solid surface, resulting in a true replication of the features of the surface, which leads to a maximized solid/solid contact area and thus strong solid/solid adhesion.

As shown in Figure 2E, when solidified paraffin wax slides on an OG surface, the total resistance force (f_{OG}) received by the wax can be contributed to by two factors: a) the viscous drag force (f_v) of the oil layer sandwiched between the solidified paraffin wax and the underlying solid surface, and b) the sliding frictional force (f_s) resulting from
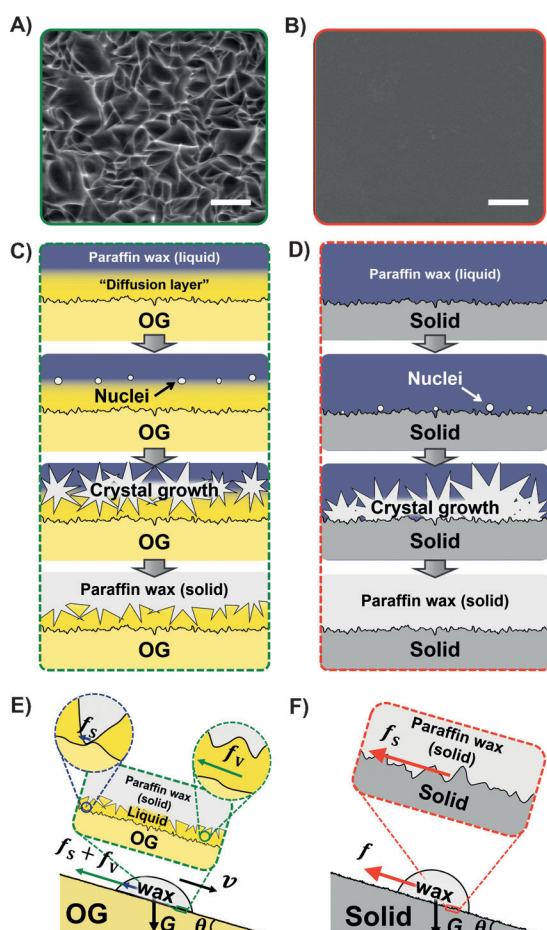
Figure 2. A) ESEM image showing the microscale structure of the solidified paraffin wax on the OG surface. B) The surface morphology of the solidified paraffin wax on the solid surface shows a true replication of the relatively smooth morphology of the solid surface. C) On the OG surface, the nucleation site is not on the cross-linked silicone surface, which leads to the formation of a rough structure. D) On the solid surface, heterogeneous nucleation takes place, resulting in growth of crystals of the paraffin wax at the solid surface. E) The structure of the OG surface gives rise to ultra-low adhesion dominated by viscous resistance, f_s, depicted by the green arrow. F) Strong wax adhesion on solid surfaces is attributed to the large contact area between the paraffin wax and the solid surface. Scale bar in (A) and (B) = 100 μm.

the solid/solid contact. As a result, the f_{OG} value can be calculated using Equation (2):

$$f_{OG} = \frac{A_a \eta_s \nu}{D} + \frac{A_r}{\delta} \Delta W \qquad (2)$$

where the first term on the right-hand side of the equation stands for the f_v parameter. A_a is the apparent contact area of the solidified paraffin wax with the surface and D is the thickness of the oil layer. The second term in Equation (2) defines the parameter $f_{s,}$ [21] where A_r is the real solid/solid contact area, δ is the interactive size of the two solids on the molecular level, and ΔW is the adhesion energy hysteresis of the two solid surfaces with ideal smoothness. Our experiment

(Figure S9) shows that as the cooling rate of the paraffin wax decreased, the shear stress for removing the solidified paraffin wax increased slightly from circa 301.3 Pa to about 1 kPa. The shear stress had a maximum of around 1 kPa for slower cooling rates. According to Equation (2), this result indicates that it is possible that the f_s term had contributed to the adhesion, but that the f_v parameter dominated the adhesion as a result of the presence of the low-molar-mass oil lubricant. It is also possible that an equilibrium exists between the wax/oil diffusion at the interface and the oil extrusion from the OG during wax solidification. The low adhesion on the OG surface is in stark contrast to adhesion on conventional surfaces. As illustrated in Figure 2F, the solidified paraffin wax could not slide because of the strong solid/solid adhesion which is expected as a result of heterogeneous nucleation initiated on the solid surface.[22]

Figure 3 shows the shear-stress test for crude-oil adhesion. In flow mode (to measure the shear stress during crude-oil flowing) shown in Figure 3B, the shear stress on the OG surface remained in the range of 0.53 ± 0.18 Pa at temperatures above 0°C and rose to circa 16.8 Pa from 0°C to −20°C. The slight increase can be expected as a result of the
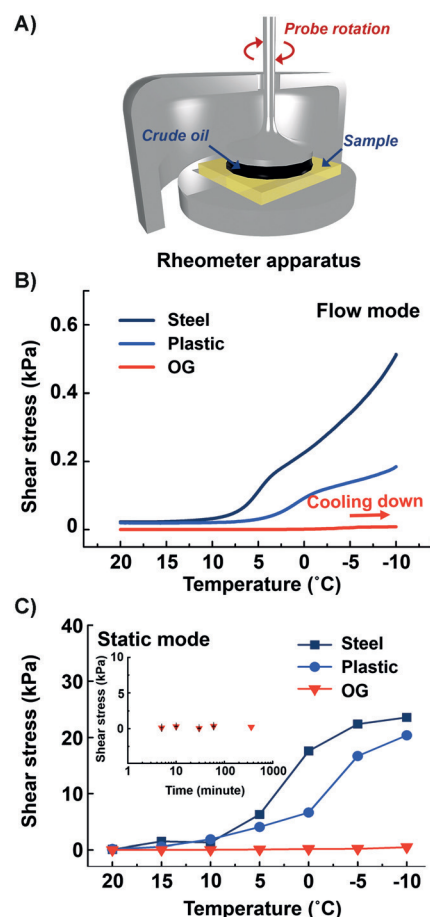

Figure 3. A) Representation of the rheometer apparatus used for shear-stress measurement at different temperatures. B) Shear stress in flow mode with decreasing temperature. C) Shear stress in static mode with decreasing temperatures. Inset in (C): the static shear stress remains almost the same with a prolonged contact time between the crude oil and the OG.

thickening of crude oil during cooling. However, the value is very small comparing to those on steel (≈ 971.2 Pa) and plastic poly(ethylene) surfaces (≈ 269.7 Pa) at $-20\,°C$, which reveals the strong potential of the OG as an inner coating material for petroleum transport tunnels.

Figure 3C shows the shear stress in static mode, which mimics the shear stress necessary to regenerate the crude-oil flow from a stationary state. Similar to flow mode, the anti-waxing performance of the OG in static mode is stable both in mild and cold temperatures, revealing the potential application of the OG material during pipeline maintenance and rebooting after emergency shutdown. However, on steel and plastic surfaces, the crude-oil adhesion strength was so strong at $-15\,°C$ and $-20\,°C$ that the crude oil fractured at the center point during rotation and so could not be removed at the crude-oil/solid interface. The inset in Figure 3C shows that the low adhesion of crude oil to the OG remains almost the same after a prolonged contact period.

Furthermore, as shown in Figure 4 the extreme situations where pipelines are fully blocked by wax plugs[4] was also
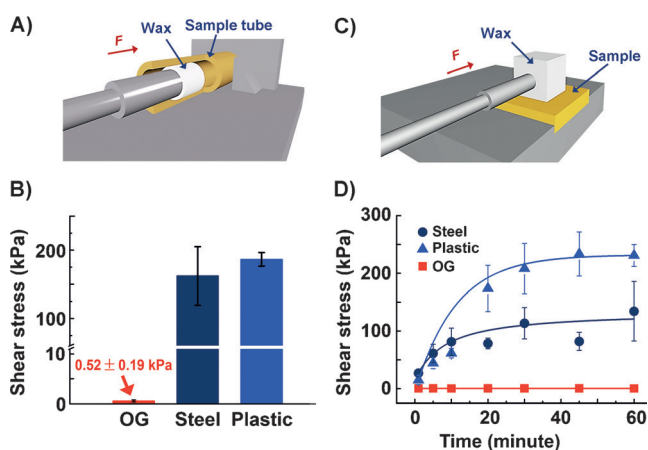
Figure 4. A) and C) Illustration of the dynamometer apparatus to test the shear stress of paraffin wax in tubes and on the surfaces of different materials. B) Tube-test results showing that the shear stress in OG tubes is more than 300 times smaller than those in steel and plastic tubes. D) The shear stress on the OG surface was very low over the time period of the test, in contrast to the significantly increasing shear stress on steel and plastic surfaces, indicating that the anti-waxing property of the OG material surface is stable as time passes.

considered. In plastic or steel tubes, the shear stress required to remove the plugs is 186.6 ± 10 kPa and 162.2 ± 42 kPa, respectively. In comparison, only 0.52 ± 0.19 kPa of shear stress was needed to remove the wax plugs when they were formed in OG tubes (Figure 4B), suggesting that the anti-waxing performance of the OG remains stable even when the pipeline is fully blocked by the wax. Figure 4D demonstrates the correlation between adhesion strength and adhesion time on different material surfaces, showing data obtained using the apparatus shown in Figure 4C. It is clear that wax adhesion on OG remained in the range of 0.4 ± 0.08 kPa and showed no increase within the time span of the test. In contrast, the shear stress reached approximately 134.2 kPa on

the steel surface and circa 233.4 kPa on plastic. This result means that the pure wax adhesion on the OG surface can be reduced by more than 500 times comparing to the plastic surface. The stable low adhesion on the OG surface indicates that the OG surface has anti-waxing properties not only at the initial stage of wax solidification, but also after being in contact with the solidified paraffin wax for an extended time period. Notably, the anti-waxing ability did not vary for a longer contact period (in hours and days) between the wax (in the liquid state) and the OG surface (Figures S10 and S11).

In summary, we have demonstrated an organogel (OG) material with ultra-low adhesion to solidified paraffin wax. In both flow and static modes, the OG shows great potential to prevent wax deposition. The fact that heterogeneous nucleation induced by the OG surface can be avoided is believed to contribute to this ultra-low adhesion. Like fish and pitcher plants utilizing water in their vicinities, the OG material is self-replenishable by absorbing the low-molar-mass components which are abundant in the crude-oil flow. It is worth mentioning that the OG material can be applied to a variety of conventional pipeline-inner-wall materials (see Figure S12 and Movies S5 and S6 in the Supporting Information for detailed experiments). In industry, solid deposition, such as scale deposition,[23] ice accumulation,[24] and FOG sedimentation in sewer systems, share the same key problem of high adhesion as a result of heterogeneous nucleation as the wax is deposited.[25] With this in mind, to deal with the issue of solid deposition in other industrial environments, the design of the OG materials developed herein can be extended to obtain gel materials with long-term durability[26] which can be self-replenishable by absorbing liquids from their vicinity.

Experimental Section

Preparation of PDMS and organogel materials: PDMS oligomer (Sylgard 184, Dow Corning) was mixed with a curing agent (ratio 10:1) to form a standard admixture. The cross-linking density of the resulting PDMS gel prepared from the standard mixture is taken as 1 unit of normalized cross-linking density (Figure S2). Similarly, the ratio of 5:1 and 20:1 are denoted as 2 units and 0.5 units, respectively. The resulting mixture was pumped under vacuum for 30 min to remove all bubbles and was placed in the oven at $80\,°C$ for 1 h. To produce the organogel, PDMS gels were immersed in different oil baths at room temperature for at least 24 h.

Shear-stress characterization using a rheometer: Generally, all samples including OG, PDMS, steel, and plastic were prepared in a uniform shape and fitted into a self-designed holder on the rheometer platform (MCR 301, Anton Paar, Austria). In flow mode (as shown in Figure 3A), crude oil (circa 1 mL) was sandwiched between the probe and the sample surface. Before operation, the chamber was kept at $20\,°C$ for more than 20 min. As probe rotation ($1\ \mathrm{rad\,min^{-1}}$) began, the temperature started to decrease from $25\,°C$ to $-20\,°C$ at a rate of $1\,°C\,\mathrm{min^{-1}}$.

In static mode, the crude oil was sandwiched between the steel probe and the sample surface at $20\,°C$. The whole system inside the chamber was maintained at a desired temperature for more than 20 min. The probe rotation ($1\ \mathrm{rad\,min^{-1}}$) did not stop until the crude oil had been sheared off the sample surface, during which time the temperature was kept constant at $20\,°C$, $15\,°C$, $10\,°C$, $5\,°C$, $0\,°C$, $-5\,°C$, and $-10\,°C$, respectively.

[1] P. Singh, R. Venkatesan, H. S. Fogler, N. Nagarajan, *Aiche J.* **2000**, *46*, 1059–1074.

[2] A. Kamari, A. H. Mohammadi, A. Bahadori, S. Zendehboudi, *Pet. Sci. Technol.* **2014**, *32*, 2837–2844.

[3] I. Procaccia, V. S. L'vov, *Rev. Mod. Phys.* **2008**, *80*, 225–247.

[4] G. Fung, W. P. Backhaus, S. McDaniel, E. M., in *Offshore Technology Conference*, Houston, Texas, USA, **2006**.

[5] a) T.-S. Wong, S. Kang, S. K. Y. Tang, E. J. Smythe, B. D. Hatton, A. Grinthal, J. Aizenberg, *Nature* **2011**, *477*, 443–447; b) T.-S. Wong, T. Sun, L. Feng, J. Aizenberg, *MRS Bull.* **2013**, *38*, 366–371; c) A. Grinthal, J. Aizenberg, *Chem. Mater.* **2014**, *26*, 698–708.

[6] a) J. D. Smith, R. Dhiman, S. Anand, E. Reza-Garduno, R. E. Cohen, G. H. McKinley, K. K. Varanasi, *Soft Matter* **2013**, *9*, 1772–1780; b) K. S. Khalil, S. R. Mahmoudi, N. Abu-dheir, K. K. Varanasi, *Appl. Phys. Lett.* **2014**, *105*, 041604; c) X. Yao, J. Ju, S. Yang, J. Wang, L. Jiang, *Adv. Mater.* **2014**, *26*, 1895–1900; d) X. Yao, S. S. Dunn, P. Kim, M. Duffy, J. Alvarenga, J. Aizenberg, *Angew. Chem. Int. Ed.* **2014**, *53*, 4418–4422; *Angew. Chem.* **2014**, *126*, 4507–4511.

[7] a) B. S. Lalia, S. Anand, K. K. Varanasi, R. Hashaikeh, *Langmuir* **2013**, *29*, 13081–13088; b) S. Anand, K. Rykaczewski, S. B. Subramanyam, D. Beysens, K. K. Varanasi, *Soft Matter* **2015**, *11*, 69–80.

[8] S. B. Subramanyam, K. Rykaczewski, K. K. Varanasi, *Langmuir* **2013**, *29*, 13414–13418.

[9] A. Lafuma, D. Quéré, *Europhys. Lett.* **2011**, *96*, 56001.

[10] a) M. Nosonovsky, *Nature* **2011**, *477*, 412–413; b) K. Rykaczewski, S. Anand, S. B. Subramanyam, K. K. Varanasi, *Langmuir* **2013**, *29*, 5230–5238.

[11] M. Liu, S. Wang, Z. Wei, Y. Song, L. Jiang, *Adv. Mater.* **2009**, *21*, 665–669.

[12] H. F. Bohn, W. Federle, *Proc. Natl. Acad. Sci. USA* **2004**, *101*, 14138–14143.

[13] H. Liu, P. Zhang, M. Liu, S. Wang, L. Jiang, *Adv. Mater.* **2013**, *25*, 4477–4481.

[14] a) F. Brochard-Wyart, P. G. de Gennes, *Macromolecules* **1977**, *10*, 1157–1161; b) S. K. Patel, C. Cohen, *Macromolecules* **1992**, *25*, 5252–5258.

[15] a) W. W. Graessley, *Polymer Liquids and Networks: Structure and Properties*, 1st ed., Garland Science, New York, **2003**; b) B. A. Miller-Chou, J. L. Koenig, *Prog. Polym. Sci.* **2003**, *28*, 1223–1270.

[16] J. L. Lenhart, P. J. Cole, *J. Adhes.* **2006**, *82*, 945–971.

[17] a) G. S. Blackman, C. M. Mate, M. R. Philpott, *Phys. Rev. Lett.* **1990**, *65*, 2270–2273; b) G. Bao, M. Troemel, S. F. Y. Li, *Appl. Phys. A* **1998**, *66*, S1283–S1288; c) M. Farshchi-Tabrizi, M. Kappl, H. J. Butt, *J. Adhes. Sci. Technol.* **2008**, *22*, 181–203.

[18] A. E. Nielsen, *Kinetics of Precipitation*, Vol. 18, Pergamon Press, Oxford, New York, **1964**.

[19] a) H. Lee, P. Singh, W. H. Thomason, H. S. Fogler, *Energy Fuels* **2008**, *22*, 480–487; b) M. Zbik, R. G. Horn, N. Shaw, *Colloids Surf. A* **2006**, *287*, 139–146; c) T. Imai, K. Nakamura, M. Shibata, *Colloids Surf. A* **2001**, *194*, 233–237.

[20] K. M. Agrawal, H. U. Khan, M. Surianarayanan, G. C. Joshi, *Fuel* **1990**, *69*, 794–796.

[21] H. Yoshizawa, Y.-L. Chen, J. Israelachvili, *J. Phys. Chem.* **1993**, *97*, 4128–4140.

[22] B. N. J. Persson, *Phys. Rev. Lett.* **2001**, *87*, 116101.

[23] M. Crabtree, D. Eslinger, P. Fletcher, M. Miller, A. Johnson, G. King, *Oilfield Rev.* **1999**, *11*, 30–45.

[24] a) R. Dou, J. Chen, Y. Zhang, X. Wang, D. Cui, Y. Song, L. Jiang, J. Wang, *ACS Appl. Mater. Interfaces* **2014**, *6*, 6998–7003; b) J. Lv, Y. Song, L. Jiang, J. Wang, *ACS Nano* **2014**, *8*, 3152–3169.

[25] a) N. P. Tung, N. Q. Vinh, N. T. P. Phong, B. Q. K. Long, P. V. Hung, *Physica B* **2003**, *327*, 443–447; b) M. Li, J. Su, Z. Wu, Y. Yang, S. Ji, *Colloids Surf. A* **1997**, *123*, 635–649.

[26] a) T. Sun, T. Kurokawa, S. Kuroda, A. B. Ihsan, T. Akasaki, K. Sato, M. A. Haque, T. Nakajima, J. Gong, *Nat. Mater.* **2013**, *12*, 932–937; b) J. Sun, X. Zhao, W. R. Illeperuma, O. Chaudhuri, K. H. Oh, D. J. Mooney, J. J. Vlassak, Z. Suo, *Nature* **2012**, *489*, 133–136; c) Q. Wang, J. L. Mynar, M. Yoshida, E. Lee, M. Lee, K. Okuro, K. Kinbara, T. Aida, *Nature* **2010**, *463*, 339–343.